

Predictive Importance Sampling Based Coverage Verification for Multi-UAV Trajectory Planning

Snehashish Ghosh and Sasthi C. Ghosh

Advanced Computing and Microelectronics Unit, Indian Statistical Institute, Kolkata, India

Email: cs2431@isical.ac.in, sasthi@isical.ac.in

Abstract—Unmanned aerial vehicle (UAV) networks are emerging as a promising solution for ultra-reliable low-latency communication (URLLC) in next-generation wireless systems. A key challenge in millimeter wave UAV networks is maintaining continuous line of sight (LoS) coverage for mobile users, as existing snapshot-based trajectory planning methods fail to account for user mobility within decision intervals, leading to catastrophic coverage gaps. Standard uniform sampling for continuous coverage verification is computationally prohibitive, requiring huge number of samples to estimate rare failure events with latencies incompatible with real-time requirements. In this work, we propose a predictive importance sampling (PIS) framework that drastically reduces sample complexity by concentrating verification efforts on predicted failure regions. Specifically, we develop a long short-term memory mixture density network (LSTM-MDN) architecture to capture multimodal user trajectory distributions and combine it with defensive mixture sampling for robustness against prediction errors. We prove that PIS provides unbiased failure probability estimates with lower variance than uniform sampling. We then integrate PIS with multi-agent deep deterministic policy gradient (MADDPG) for coordinated multi-UAV trajectory planning using an adaptive multi-objective reward function balancing throughput, coverage, fairness, and energy consumption. Lastly, the simulation results show how our suggested method outperforms three other state-of-the-art methods in terms of coverage rate, throughput, and verification latency, making proactive coverage management for URLLC-aware UAV networks feasible.

Index Terms—Importance sampling, Coverage verification, URLLC, LSTM-MDN, Coordinated trajectory planning.

I. INTRODUCTION

Unmanned aerial vehicle (UAV) networks have become a versatile way to handle ultra-reliable low-latency communication (URLLC) needs, such as emergency services, industrial IoT, and autonomous vehicles alongside enhanced mobile broadband (eMBB) services for high-throughput data-intensive applications [1], [2]. While eMBB users can tolerate minor delays, URLLC users require sub-millisecond latency and very high reliability, which means the network must be managed proactively instead of just reacting to the problems. Over short distances, millimeter-wave (mmWave) can provide high data speeds and dependability. However, due to substantial propagation and penetration losses of mmWave, line-of-sight (LoS) conditions are the main factor in link quality, so maintaining a steady LoS connection is vital for users on the move [3]. Plenty of research focuses on where to put UAVs [5] and how to plan their paths [4] to maximize coverage. Recent studies use deep reinforcement learning like multi-agent deep deterministic policy gradient (MADDPG) for coordinating multiple UAVs trajectory planning [7], [14]. While these methods

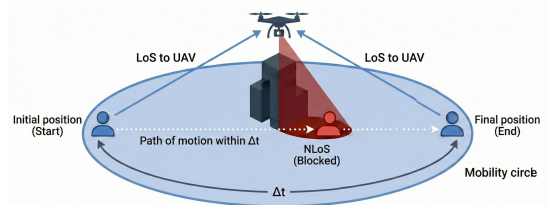


Fig. 1. Analysis of coverage gaps during user movement.

achieve effective trajectory planning, their coverage verification mechanisms have critical limitations. Qin et al. [11] verify coverage through SINR thresholds and queue-based URLLC constraints, but only at discrete time slots under quasi-static assumptions. Dhinesh Kumar et al. [13] use binary coverage indicators that check if data rates exceed thresholds at specific checkpoints, achieving good snapshot-based verification. However, all these approaches share a fundamental limitation, they only verify coverage at discrete time points and ignore what happens during user movement within decision intervals Δt . This creates a critical gap where users with LoS at times t and $t + \Delta t$ may still experience intermediate non-LoS (NLoS) due to obstacles during movement. These methods lack predictive mechanisms to anticipate where failures are likely to occur, leading to inefficient allocation of computational resources. More precisely, a user's LoS connectivity with the UAV at the start and finish of that time interval does not always imply LoS connectivity throughout the duration of that period. (Fig. 1). This leads to dropped connections, which can be devastating for delay-sensitive URLLC based mission critical applications as well as makes a system less reliable for eMBB users. It can be addressed by considering users' location at very short intervals by making Δt very small. However, in that case, location updates will take up a significant portion of data communication time, thereby reducing the user throughput substantially.

If no past mobility related information is considered, at a particular time point t , a user u positioned at u_t and moving at velocity v can end up anywhere inside the mobility circle of radius $v \cdot \Delta t$ with center as u_t . To ensure complete coverage, we should confirm that no point within C falls into NLoS. Checking every point via ray-casting is impossible. Instead, we have to use probabilistic estimation to find the failure probability P_f . For high reliability, P_f must be very small. Using standard uniform Monte Carlo estimation, $N = O(1/\sqrt{P_f})$ samples are required [15] implying approximately 10^6 samples

for $P_f = 10^{-4}$. Assuming that each sample takes about $1\mu\text{s}$ for ray-casting, this corresponds to a latency of roughly 1 to 100 ms per user. This is too slow for a real-world system that requires sub-millisecond latency.

One way to reduce this latency is to consider the past mobility related information of the users. Long short-term memory (LSTM) networks are great for modeling this type of past information sequences [16]. However, predicting a single deterministic trajectory introduces significant uncertainty as the users at intersections can take multiple possible paths, and averaging these possibilities often yields physically unrealistic predictions. To address this, mixture density networks (MDNs) [17] can be integrated with LSTMs to model the inherent multimodality of user movement, predicting multiple possible trajectories with associated probabilities. Moreover, by sampling preferentially in these high-probability directions rather than uniformly throughout the entire mobility region C , more efficient coverage verification can be achieved. Such non uniform sampling can efficiently be modeled by using classical *importance sampling* (IS).

To the best of our knowledge, no existing research covers (1) efficient coverage checking for continuous movement between timesteps, (2) combining learned path prediction with formal IS theory, or (3) real-time coordination for multiple UAVs with lower variance. Building on these insights, we develop a predictive importance sampling (PIS) which provably reduces variance in Monte Carlo estimation [9], [15] and consequently reduces verification latency by focusing computational resources on the most critical regions. Using this, we develop an efficient multi-UAV trajectory planning mechanism. More specifically our contributions can be summarized as follows:

- 1) We develop a theoretically-grounded PIS framework for efficient coverage verification, and prove that it provides unbiased failure probability estimates with reduced variance versus uniform sampling under specified conditions. Unbiasedness ensures accurate URLLC reliability guarantees, while variance reduction enables real-time verification with significantly fewer samples.
- 2) We create an LSTM-MDN architecture as the predictive foundation that generates multi-modal trajectory distributions focusing sampling on anticipated failure locations, employing a defensive mixture approach combining prediction with uniform sampling backup for robustness.
- 3) We develop an adaptive multi-objective reward function with learnable weights that dynamically balances throughput, coverage, fairness, and energy efficiency based on network state.
- 4) We integrate PIS with MADDPG to design coordinated multi-UAV trajectory planning enabling real-time proactive coverage management, and establish our strategy's superiority over state-of-the-art approaches through comprehensive experiments.

The rest of this paper is organized as follows: Section II describes the system model, Section III presents the proposed

PIS framework along with its proofs of unbiasedness and variance reduction, LSTM-MDN architecture, and coordinated multi-UAV trajectory planning, Section IV provides simulation results and comparison with existing related strategies, and Section V concludes with possible future directions.

II. SYSTEM MODEL

A. Network Topology

We consider a three-dimensional air-to-ground cellular wireless communication system consisting of N_{UAV} UAVs serving as aerial base stations and N_{users} ground users over a geographical area of $a \times a \text{ m}^2$. Here, both UAVs and users are mobile. The environment contains M static obstacles (buildings) that can block LoS paths between UAVs and ground users. Each UAV operates within an altitude range of h_{min} to h_{max} meters with maximum speed v_{UAV} m/s to avoid collision with buildings as well to ensure *safe flight zone* within the designated green zone. We assume ground users are located at zero altitude. Time is discretized into decision intervals of duration Δt seconds.

B. Channel Model

We adopt the 73 GHz air-to-ground propagation model with both LoS and NLoS conditions. The path loss (in dB) for the link between UAV i and user j is [10]:

$$PL_{i,j}(d_{i,j}) = \alpha_{pl} + 10\beta_{pl} \log_{10}(d_{i,j}), \quad (1)$$

where α_{pl} and β_{pl} are environment-specific constants and $d_{i,j}$ is the Euclidean distance. The received power (in dBm) at user j from UAV i is:

$$P_{i,j} = P_i + G_i + G_j - PL_{i,j}(d_{i,j}), \quad (2)$$

where P_i is the transmit power and G_i , G_j are antenna gains at the UAV and user, respectively. The achievable throughput is given by Shannon's capacity [10]:

$$T_{i,j} = B_w \log_2 \left(1 + \frac{P_{i,j} \times |g_{i,j}|^2}{\sigma_0^2} \right), \quad (3)$$

where B_w is the channel bandwidth, σ_0^2 is the additive white Gaussian noise power, and $|g_{i,j}|$ is the small-scale fading coefficient following Rician (LoS) or Rayleigh (NLoS) distributions.

C. User Traffic Characterization

According to user delay tolerance requirements, we classify users into two service classes namely URLLC and eMBB. For simplicity we have not considered massive machine-type communication (mMTC) users as we focus only on human type applications. URLLC traffic is designed for mission-critical applications requiring sub-millisecond latency and high reliability. Even minor coverage interruptions during user movement can cause catastrophic failures. URLLC users require continuous LoS coverage verification throughout their mobility region during decision interval Δt . A user is considered covered if the estimated failure probability \hat{P}_f below a pre-defined threshold. eMBB traffic has been designed for high-throughput, data-intensive applications that can tolerate minor delays. eMBB users do not require extensive LoS coverage verification.

D. Mobility Model

User velocities are bounded by $v_u \in [0, v_{max}]$ m/s, representing pedestrian and vehicular mobility. Users remain within the simulation area through boundary reflection. At a particular time point $t \in [0, \Delta t]$, a user at position u_t with velocity v_u can occupy any position within the mobility circle:

$$C = \{z \in \mathbb{R}^2 : \|z - u_t\| \leq r\}. \quad (4)$$

where $r = v_u \cdot \Delta t$. UAVs execute continuous control actions $\Delta p = (\Delta x, \Delta y, \Delta z)$ generated by actor networks, constrained by the velocity $v_{uav} \in [0, V_{max}]$ m/s. Position updates are:

$$p_{t+1} = p_t + v_{uav} \cdot \Delta t, \quad (5)$$

with hard boundary constraints ensuring UAVs remain within the safe flight zone.

III. PROPOSED STRATEGY

This section presents our predictive importance sampling framework for efficient user coverage verification in UAV networks. We formulate the rare event challenge (III-A), introduce importance sampling principles and derive the optimal proposal distribution (III-B), then present our practical PIS model combining LSTM-based trajectory prediction with defensive mixture sampling using MDN (III-C). We prove the unbiasedness and variance reduction properties of our estimator (III-D), describe the LSTM-MDN architecture for multimodal trajectory prediction (III-E), and present MADDPG-based coordinated multi-UAV planning with adaptive multi-objective rewards (III-F).

A. Rare Event Challenge

As mentioned earlier unlike eMBB, URLLC requirements mandate continuous coverage throughout C . Formally, we must verify $L(z) = 1$ for all $z \in C$, where $L(z)$ denotes the LoS status of the point z . Since verifying uncountably infinite points is intractable, we estimate failure probability. Assuming worst-case uniform uncertainty over C , the failure probability is:

$$P_f = \frac{\int_C I_F(z) dz}{\int_C dz} = \mathbb{E}_p[I_F(Z)], \quad (6)$$

where $Z \sim \text{Uniform}(C)$, $p(z) = 1/A$ with A being the area of the mobility circle C and $I_F(z) = 1(0)$ is the indicator variable showing the NLoS (LoS) at position z . Standard Monte Carlo estimator is

$$\hat{P}_f^{\text{uniform}} = \frac{1}{N} \sum_{i=1}^N I_F(Z_i), \quad Z_i \sim \text{Uniform}(C). \quad (7)$$

Now we come across the *rare event challenge* where probability of NLoS is very rare which may require extraordinary effort to locate the NLoS. To address this rare event challenge we adopt the importance sampling principle.

B. Importance Sampling (IS) Principles

IS is a variance reduction technique that changes the sampling distribution while maintaining unbiasedness through impor-

tance weights [9]. The fundamental IS identity states that for any expectation $\mu = \mathbb{E}_p[f(X)]$ under distribution $p(x)$:

$$\mu = \int f(x)p(x) dx = \mathbb{E}_q \left[f(X) \frac{p(X)}{q(X)} \right] \quad (8)$$

where $q(x)$ is any proposal distribution with support containing that of $p(x)$. The term $w(x) = p(x)/q(x)$ is the importance weight. The IS estimator is [15]:

$$\hat{\mu}_q = \frac{1}{N} \sum_{i=1}^N f(X_i)w(X_i), \quad X_i \stackrel{\text{i.i.d.}}{\sim} q(x). \quad (9)$$

This estimator is *unbiased* meaning its expected value is equal to the true mean μ , provided the support condition $q(x) > 0$ wherever $p(x) > 0$ is met [15]. The proof is a direct consequence of the IS identity:

$$\mathbb{E}_q[\hat{\mu}_q] = \mathbb{E}_q[f(X)w(X)] = \mu. \quad (10)$$

Its variance is:

$$\text{Var}_q(\hat{\mu}_q) = \frac{1}{N} [\mathbb{E}_q[(f(X)w(X))^2] - \mu^2]. \quad (11)$$

If $f(x) \geq 0$ for all x , the *optimal proposal distribution* that minimizes variance is:

$$q^*(x) = \frac{f(x)p(x)}{\int f(y)p(y) dy} = \frac{f(x)p(x)}{\mu} \quad [15]. \quad (12)$$

Based on IS principles, we now propose an intelligent predictive importance sampling (PIS) model for coverage verification.

C. Proposed PIS model for Coverage Verification

For our coverage verification problem, we have $f(x) = I_F(x)$. Since $I_F(x) \in \{0, 1\}$, the condition $f(x) \geq 0$ for the optimal proposal distribution in (12) is satisfied. If $f(x) = I_F(x)$, $f(x)w(x) = f(x) \frac{p(x)}{q^*(x)} = \mu$ implying that variance as stated in (11) becomes zero. However, as we can see from (12), constructing q^* requires knowing μ itself, the very quantity we seek to estimate. Therefore, practical IS designs $q(x)$ to approximate $q^*(x)$. In our coverage verification problem, $f = I_F$ and p is uniform implying $p(x) = 1/A$. Since μ is constant, from (11), we get $q^*(z) \propto I_F(z)$. This implies that the optimal proposal concentrates samples on NLoS regions. Note that our objective is to design the learned $q(z)$ to approximate $q^*(z)$. A critical failure will occur when $q(z) \approx 0$ where $p(z) > 0$. This causes importance weights $w(z) = p(z)/q(z) \rightarrow \infty$, implying a catastrophic increase in variance. This is particularly dangerous with learned proposals that may mis-predict failure (NLoS) regions. To overcome this, we employ a defensive mixture strategy:

$$q_{\text{pis}}(z) = \alpha \cdot q_{\text{pred}}(z) + (1 - \alpha) \cdot p(z), \quad \alpha \in [0, 1] \quad (13)$$

where $q_{\text{pred}}(z)$ is the LSTM-MDN prediction concentrating on predicted failure regions and $p(z)$ is the uniform distribution ensuring *fallback coverage*. Since $p(z) = 1/A > 0$ everywhere in C , we have $q_{\text{pis}}(z) \geq (1 - \alpha)/A > 0$ for all $z \in C$, guaranteeing bounded importance weights $w(z) \leq A/(1 - \alpha)$. Here the parameter α provides tunable control: higher the α (tends to 1) more is the reliance on prediction whereas low α

(tends to 0) prioritizes robust uniform coverage. So, α must be chosen empirically to balance both the objectives.

D. Proof of Unbiasness and Variance Reduction of PIS

Theorem 1. *The PIS estimator*

$$\hat{P}_{PIS} = \frac{1}{N} \sum_{i=1}^N I_F(Z_i) \frac{p(Z_i)}{q_{pis}(Z_i)}, \quad Z_i \stackrel{i.i.d.}{\sim} q_{pis} \quad (14)$$

is unbiased: $\mathbb{E}_{q_{pis}}[\hat{P}_{PIS}] = P_f$.

Proof. By linearity of expectation and i.i.d. samples:

$$\mathbb{E}_{q_{pis}}[\hat{P}_{PIS}] = \mathbb{E}_{q_{pis}} \left[I_F(Z) \frac{p(Z)}{q_{pis}(Z)} \right] \quad (15)$$

$$= \int_C I_F(z) \frac{p(z)}{q_{pis}(z)} q_{pis}(z) dz \quad (16)$$

$$= \int_C I_F(z) p(z) dz = \mathbb{E}_p[I_F(Z)] = P_f \quad (17)$$

where $q_{pis}(z)$ terms cancel since $q_{pis}(z) > 0 \forall z$. \square

Theorem 2. *Let $\mathcal{F} = \{z \in C : I_F(z) = 1\}$ be the failure region. If $q_{pis}(z) \geq p(z)$ for all $z \in \mathcal{F}$, then:*

$$\text{Var}_{q_{pis}}(\hat{P}_{PIS}) \leq \text{Var}_p(\hat{P}_{uniform}) \quad (18)$$

Proof. The variance of the uniform estimator is:

$$\begin{aligned} \text{Var}_p(\hat{P}_{uniform}) &= \frac{1}{N} [\mathbb{E}_p[I_F(Z)^2] - P_f^2] \\ &= \frac{1}{N} [P_f - P_f^2] = \frac{P_f(1 - P_f)}{N}, \end{aligned} \quad (19)$$

since $I_F(Z)^2 = I_F(Z)$ for binary indicators.

The variance of the PIS estimator is:

$$\text{Var}_{q_{pis}}(\hat{P}_{PIS}) = \frac{1}{N} [\mathbb{E}_{q_{pis}}[(I_F(Z)w(Z))^2] - P_f^2]. \quad (20)$$

For variance reduction, we require $\text{Var}_{q_{pis}} \leq \text{Var}_p(\hat{P}_{uniform})$. Therefore, after equating (19) & (20) we get:

$$\mathbb{E}_{q_{pis}}[(I_F(Z)w(Z))^2] \leq P_f. \quad (21)$$

Converting to expectation over p :

$$\begin{aligned} \mathbb{E}_{q_{pis}}[(I_F w)^2] &= \int_C I_F(z)^2 w(z)^2 q_{pis}(z) dz \\ &= \int_C I_F(z) \frac{p(z)^2}{q_{pis}(z)} dz \\ &= \mathbb{E}_p \left[I_F(Z) \frac{p(Z)}{q_{pis}(Z)} \right]. \end{aligned} \quad (22)$$

So, the variance reduction holds if and only if:

$$\mathbb{E}_p \left[\frac{I_F(Z)p(Z)}{q_{pis}(Z)} \right] \leq \mathbb{E}_p[I_F(Z)] = P_f. \quad (23)$$

We now show that the pointwise condition $q_{pis}(z) \geq p(z)$ for all $z \in \mathcal{F}$ is sufficient to guarantee (23).

Now, if $q_{pis}(z) \geq p(z)$ holds for all $z \in \mathcal{F}$, then we get $\frac{p(z)}{q_{pis}(z)} \leq 1$. Since $I_F(z) = 0$ for all $z \notin \mathcal{F}$, we have:

$$I_F(z) \frac{p(z)}{q_{pis}(z)} \leq I_F(z) \quad \text{for all } z \in C \quad (24)$$

Taking expectations with respect to $p(z)$:

$$\mathbb{E}_p \left[I_F(Z) \frac{p(Z)}{q_{pis}(Z)} \right] \leq \mathbb{E}_p[I_F(Z)] = P_f \quad (25)$$

This establishes (23), completing the proof. \square

Theorems 1 and 2 provide a clear design principle that the predictive model q_{pred} must concentrate sufficient probability mass on failure regions such that $q_{pis}(z) \geq p(z)$ for all $z \in C$ holds. If the model q_{pred} accurately identifies NLoS areas, this condition is satisfied, yielding variance reduction. If it cannot do so, the variance may exceed uniform sampling, however, it remains *bounded* and controllable via α .

E. Trajectory Prediction using LSTM-MDN Architecture

To determine the optimal proposal distribution $q^* \propto I_F(z)$, we must accurately predict user locations and NLoS regions by modeling their historical movement. User movement exhibits strong trends. At time t , we observe H sequences of historical velocity data $\{(\mathbf{v}_{x,t-H}, \mathbf{v}_{y,t-H}), \dots, (\mathbf{v}_{x,t-1}, \mathbf{v}_{y,t-1})\}$ and feed them into a 2-layer LSTM with hidden dimension 128, capturing movement patterns in the final hidden state h_t . Standard networks predict a single trajectory, but real-world user movement is multimodal with multiple possible directions. For example, a user at a street corner can turn left, right, or continue straight, averaging these yields physically unrealistic predictions (e.g., walking into a building). MDNs [17] solve this by outputting Gaussian mixture model (GMM) parameters instead of a single prediction. The MDN computes K possible paths using LSTM state h_t : mixture weights $\pi_k(h_t)$ (summing to 1), mean positions $\boldsymbol{\mu}_k(h_t) \in \mathbb{R}^2$, and covariances $\boldsymbol{\Sigma}_k(h_t) \in \mathbb{R}^{2 \times 2}$. The predictive distribution is:

$$q_{pred}(z|h_t) = \sum_{k=1}^K \pi_k(h_t) \mathcal{N}(z|\boldsymbol{\mu}_k(h_t), \boldsymbol{\Sigma}_k(h_t)). \quad (26)$$

The model is trained using negative log-likelihood (NLL) loss. The architecture comprises an input layer (velocity sequences of size $H \times 2$), a 2-layer LSTM, and an MDN output head with softmax functions on weights π_k , linear functions on means $\boldsymbol{\mu}_k$, and exponential functions ensuring positive diagonal covariance.

We now present **Algorithm 1** which computes PIS failure probability. It begins by processing the user's velocity history \mathcal{H}_v via the LSTM-MDN to generate trajectory predictions. A defensive mixture proposal $q_{pis}(z)$ is constructed to ensure sampling robustness. The core loop executes IS: it draws samples from q_{pis} , verifies LoS, and computes importance weights. The aggregated failure probability \hat{P}_f is then thresholded against ϵ to output a binary coverage quality metric Q_u . This Q_u serves as the statistically verified ground truth for the reward function in the next stage. Complexity of Algorithm 1 is $O(N \cdot C_{los}) \approx O(N)$, where N is the sample count and C_{los} is the cost of LoS check (typically $O(1)$ with height maps).

Until now we assumed single UAV for user trajectory prediction through coverage failure estimation. In order to

Algorithm 1 PIS Failure Probability Estimation

Input: User state u_t , Velocity history \mathcal{H}_v , Sample count N , mixture weight α .

Output: Binary coverage Quality Q_u .

- 1: **Predict:** Get parameters $\{\pi_k, \mu_k, \Sigma_k\} \leftarrow \text{LSTM-MDN}(\mathcal{H}_v)$
 - 2: **Construct Proposal:** $q_{pis}(z) = \alpha \sum \pi_k \mathcal{N}(z|\mu_k, \Sigma_k) + (1 - \alpha)U(\mathcal{C})$ {Where $U(\mathcal{C})$ is Uniform PDF: $1/\text{Area}(\mathcal{C})$ }
 - 3: Initialize weighted failure sum $W_{fail} \leftarrow 0$
 - 4: **for** $i = 1$ to N **do**
 - 5: Sample potential user location $z_i \sim q_{pis}(z)$
 - 6: Reject if $\|z_i - u_t\| > \text{Radius}(\mathcal{C})$ (ensure $z_i \in \mathcal{C}$)
 - 7: Check Line-of-Sight: $I_F(z_i)$
 - 8: **if** $I_F(z_i) == 1$ **then**
 - 9: Compute Importance Weight: $w_i \leftarrow \frac{1/\text{Area}(\mathcal{C})}{q_{pis}(z_i)}$
 - 10: $W_{fail} \leftarrow W_{fail} + w_i$
 - 11: **end if**
 - 12: **end for**
 - 13: Estimate Failure Prob: $\hat{P}_f \leftarrow W_{fail}/N$
 - 14: Determine Quality: **if** $\hat{P}_f < \epsilon$ **then** $Q_u \leftarrow 1$ (Success) **else** $Q_u \leftarrow 0$ (Failure)
 - 15: **return** Q_u
-

avoid collisions and a significant overlap of served users, we suggest using multiple UAVs with coordinated operations. In the next subsection, we use multiple UAVs as agents and employ MADDPG [14] to coordinate the operations.

F. Coordinated Multi-UAV Trajectory Planning

MADDPG uses centralized training with decentralized execution. We have designed a multi-objective reward function for proactive coverage maintenance:

$$R_t = \sum_{j \in R} \omega_j \cdot \Phi_j(R_j) + \sum_{k \in P} \omega_k \cdot \Phi_k(P_k), \quad (27)$$

where $\Phi(\cdot)$ is a normalization function representing the rewards $R = \{\text{throughput}, \text{coverage}, \text{load balance}\}$ and penalties $P = \{\text{energy}, \text{collision}\}$. We have normalized each objective against its theoretical capacity or statistical maximum, transforming all components into dimensionless utility ratios $\in [0, 1]$ [6]. We now define all the rewards (R) and penalties (P) where user is denoted by u and UAV is denoted by i .

Normalized *throughput* reward:

$$\Phi_{\text{thr}}(R_{\text{thr}}) = \frac{\sum_{(i,u)} B \log_2(1 + \text{SNR}_{i,u})}{N_{\text{users}} \cdot B \cdot \log_2(1 + \text{SNR}_{\text{max}})}, \quad (28)$$

where $\text{SNR}_{\text{max}} = P_{\text{tx}} \cdot g(h_{\text{min}})/N_0$ is the theoretical maximum at minimum altitude.

Normalized *coverage* reward:

$$\Phi_{\text{cov}}(R_{\text{cov}}) = \frac{\sum_u w_u \cdot Q_u}{\sum_u w_u}, \quad (29)$$

where Q_u is a binary coverage quality variable indicating accurate failure probability estimation. Computation of Q_u is shown in Algorithm 1.

Normalized *load balance* reward:

$$\Phi_{\text{bal}}(R_{\text{bal}}) = \frac{\bar{n} - \sigma_n}{\bar{n} + \epsilon}, \quad (30)$$

where \bar{n} is mean user count per UAV and σ_n is standard deviation.

Normalized *energy consumption* penalty:

$$\Phi_{\text{energy}}(P_{\text{energy}}) = 1 - \frac{\sum_i \|\Delta \mathbf{p}_i\|}{N_{\text{UAV}} \cdot v_{\text{max}} \cdot \Delta t}, \quad (31)$$

Normalized *collision* penalty:

$$\Phi_{\text{coll}}(P_{\text{coll}}) = \frac{1}{N_{\text{pairs}}} \sum_{i < j} \exp\left(-\frac{|d_{ij} - d_{\text{shift}}|}{k_{\text{scale}}}\right), \quad (32)$$

where N_{pairs} is the number of UAV pairs, d_{ij} is the distance between the UAVs i and j and d_{shift} and k_{scale} denote the appropriate shifting and scaling parameters.

Rather than manually tuning the weights ω_i , we employ a learnable weight network $\pi_\omega : \mathcal{S} \rightarrow \Delta^4$, where Δ^4 is 5-dimensional probability simplex that dynamically adjusts priorities of the reward components based on global state.

Algorithm 2 discusses the integration of above computed reward function and uses centralized training decentralized execution (CTDE) for coordinated trajectory planning. At the start of an episode, the weight network π_ω analyzes the global state to adaptively set objective priorities ω (Line 3). During execution, Line 8 calls Algorithm 1 to compute Q_u for every user. This value feeds directly into the normalized coverage reward Φ_{cov} (Line 11), which is aggregated with throughput, load balance, and safety penalties into the global reward R_t . Coordination is enforced during the training phase (Line 15), where the centralized critic Q_i updates based on the *joint* actions of all UAVs, effectively learning to penalize non-cooperative behaviors like collisions or redundant coverage. The computational complexity of Algorithm 2 is analyzed below. Let $J = |\mathcal{I}|$ denote the number of UAV agents, K_{URLLC} denote the number of URLLC users requiring PIS verification, and N denote the number of importance samples per user in Algorithm 1. The actor μ and critic Q networks have L_μ and L_Q layers respectively, where the l -th layer of the actor network has U_l neurons and the m -th layer of the critic network has V_m neurons. The weight network π_ω has $|\pi_\omega|$ parameters. Therefore, the training complexity is $\mathcal{O}(M \cdot T \cdot (J^2 |\mathcal{B}| \sum_{l=1}^{L_\mu} U_{l-1} U_l + J |\mathcal{B}| \sum_{m=1}^{L_Q} V_{m-1} V_m + J \cdot K_{\text{URLLC}} \cdot N))$, where $|\mathcal{B}|$ is the mini-batch size. The deployment complexity is $\mathcal{O}(T \cdot (J \sum_{l=1}^{L_\mu} U_{l-1} U_l + J \cdot K_{\text{URLLC}} \cdot N)) = \mathcal{O}(T \cdot (J |s| |a| + J \cdot K_{\text{URLLC}} \cdot N))$, where $|s|$ and $|a|$ are the dimensions of state and action, respectively.

IV. SIMULATION RESULTS

We compare our proposed scheme (MADDPG-PIS) with three other schemes. MADDPG [14], which is a multi-agent actor-critic framework addressing environmental non-stationarity by incorporating the policies of other agents into a centralized critic. SAC [11], which is an off-policy soft actor-critic algorithm designed to maximize computation throughput jointly optimizing UAV trajectories and beamforming while maintaining

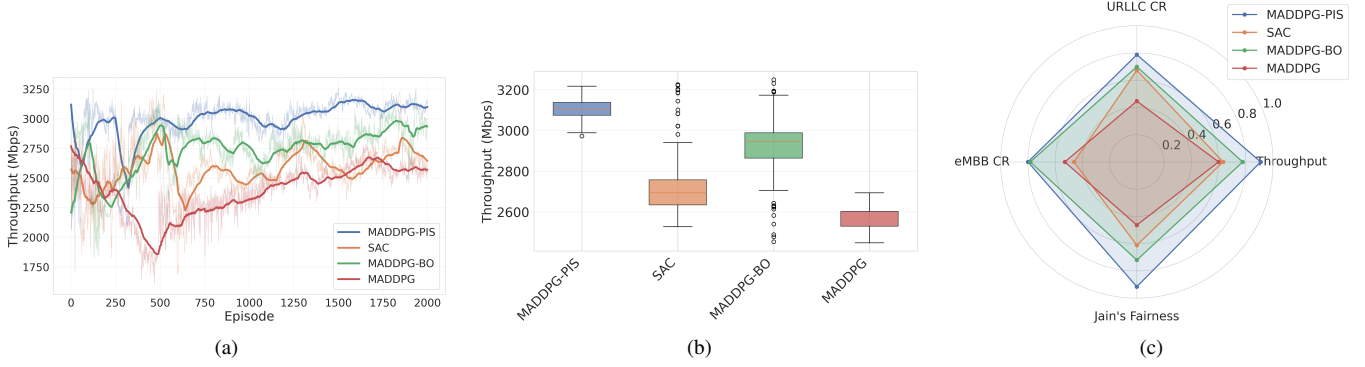


Fig. 2. (a) Episode-wise throughput(Mbps) (b) Throughput(Mbps) distribution (final 200 episodes) (c) Normalized performance comparison.

Algorithm 2 PIS-Guided Multi-UAV Trajectory planning

Input: Agents \mathcal{I} , Env \mathcal{E} , WeightNet π_ω , Actor μ , Critic Q .

- 1: **for** episode $ep = 1$ to M **do**
- 2: Observe joint state $\mathbf{s} = \{s_1, \dots, s_N\}$
- 3: Get adaptive weights: $\omega \leftarrow \pi_\omega(\mathbf{s}_{global})$
- 4: **for** step $t = 1$ to T **do**
- 5: Select actions $\mathbf{a}_t = \{\mu_i(s_i) + \mathcal{N}_t\}_{i \in \mathcal{I}}$
- 6: Execute actions: $\mathbf{s}' \leftarrow \text{Step}(\mathbf{a}_t)$
- 7: **for** each UAV $i \in \mathcal{I}$ **do**
- 8: Call Alg. 1 for assigned users to get Q_u
- 9: **end for**
- 10: Calculate Normalized Components [Eq. (28)- (32)]:
 Φ_{thr}, Φ_{cov} (via Q_u), $\Phi_{bal}, \Phi_{eng}, \Phi_{col}$.
- 11: Compute Global Reward: $R_t \leftarrow \sum \omega_j \Phi_j + \sum \omega_k \Phi_k$
- 12: Store transition $\langle \mathbf{s}, \mathbf{a}, R_t, \mathbf{s}' \rangle$ in Replay Buffer \mathcal{D}
- 13: Sample batch \mathcal{B} from \mathcal{D}
- 14: **Coordination:** Update Critic Q_i using Joint Actions $\mathbf{a}_{1..M}$ and State \mathbf{S}_{global}
- 15: Update Actors μ_i via deterministic policy gradient
- 16: Update WeightNet π_ω to max long-term utility
- 17: Update states: $\mathbf{s} \leftarrow \mathbf{s}'$
- 18: **end for**
- 19: **end for**
- 20: **end for**

URLLC awareness and training stability. MADDPG-BO [13], which is an enhanced multi-agent approach that integrates Bayesian optimization for efficient hyperparameter tuning to optimize UAV trajectories, trying to improve coverage in rural and urban environments. Moreover, we consider uniform-1000 which is a uniform sampling with $N = 1000$ as accuracy baseline. The simulation parameters we have used in the process are listed in Table I.

Fig. 2 and Table II present a comprehensive evaluation of the proposed MADDPG-PIS framework against baseline methods across convergence, stability, and multi-objective performance dimensions. The episode-wise throughput trajectories in Fig. 2a) reveal learning dynamics over 2000 training episodes. Raw measurements (transparent lines) exhibit inherent stochastic variance, while the smoothed curves high-

TABLE I
SIMULATION PARAMETERS

Parameter	Value
Simulation area ($a \times a m^2$)	1500m \times 1500m
Number of users (N_{users})	30 (URLLC), 200 (eMBB)
Number of UAVs (N_{UAV})	5
UAV communication range	300 m
Decision interval (Δt)	10 sec
Transmission power (P_i)	30 dBm [21]
UAV maximum speed (v_{max})	30 m/s [13]
Mixture weight (α)	0.6
LSTM hidden dimension(h_t)	128
Buffer size	50000
Rician fading factor	2 [11]
Altitude of UAV	[22 m, 150 m] [20]
Carrier frequency	73 GHz [21]
LoS link parameters	$\alpha_{pl} = 69.8, \beta_{pl} = 2, \sigma_0 = 3.1$ [21]

TABLE II
PERFORMANCE COMPARISON

Method	Throughput (Mbps)	URLLC CR(%)	eMBB CR(%)	Energy (kJ)	Jain's index
Proposed method	3127.85	74.1	61.7	116.1	0.71
MADDPG+BO	2906.49	64	59.8	123.6	0.61
SAC	2724.62	63.8	51.5	130.3	0.59
MADDPG	2563.03	55.2	51.5	92.1	0.52

light convergence trends. MADDPG-PIS demonstrates superior asymptotic performance, converging to ~ 3100 Mbps by episode 1500. Notably, MADDPG exhibits prolonged initial instability (episodes 0-500) before gradual convergence, whereas PIS-guided exploration accelerates early-stage learning due to optimistic initialization. Box plots (Fig. 2b) characterize steady-state performance distributions over the final 200 episodes. The interquartile range (IQR) quantifies policy stability where MADDPG-PIS exhibits the tightest distribution (IQR = 62.89 Mbps), indicating consistent performance with minimal variance. In contrast, SAC, MADDPG-BO, MADDPG has IQR (Mbps), 123.43, 124.57 and 73.76 respectively. The median line position within each box confirms that MADDPG-PIS maintains higher central tendency without extreme deviations. The radar chart (Fig. 2c) normalizes four critical metrics to [0,1] for comparative visualization. MADDPG-PIS achieves

the largest enclosed area, demonstrating balanced excellence across multiple competing objectives. Specifically, it dominates in throughput, URLLC coverage ratio and Jain’s Fairness index, while maintaining eMBB coverage. The rhomboid shape of baseline MADDPG reveals its bias toward lower fairness at the expense of reliability. MADDPG-BO shows improved coverage over SAC but lags in fairness index. Absolute performance metrics over converged episodes (Table II) confirm MADDPG-PIS has an upper hand: 3127.85 Mbps throughput (+22% vs. vanilla MADDPG, +14.8% vs. SAC and +7.6% vs. MADDPG-BO), 74.1% URLLC CR (+10.3% vs. MADDPG-BO), and 0.71 Jain’s index (+16.4% vs. MADDPG-BO).

Table III presents our ablation study. The proposed ($\alpha = 0.6, N = 100$) achieves optimal performance (3097 Mbps, 72% URLLC CR, 0.57 ms latency) with estimator variance 5.2×10^{-5} , marginally higher than Uniform ($N = 1000$) at 4.8×10^{-5} . This is expected since Theorem 2 guarantees variance reduction at equal N , not across different sample budgets. Notably, the $10\times$ sample reduction causes only a marginal increase rather than proportional increase that naive uniform subsampling would incur, empirically demonstrating PIS’s superior per-sample efficiency. High $\alpha = 0.9$ degrades throughput to 2219 Mbps and 50.6% CR as insufficient uniform fallback exposes prediction errors, with inflated variance (29.8×10^{-5}) reflecting unbounded importance weights under MDN misprediction. Low $\alpha = 0.3$ under-utilizes prediction, yielding 2376 Mbps and 52.8% CR with variance (19.1×10^{-5}) as the uniform fallback dominates. Uniform ($N = 1000$) achieves comparable accuracy but at 11 ms latency which is $20\times$ slower than PIS thereby rendering it impractical for real-time control.

The convergence of evidence across visualization modalities establishes that PIS-guided coverage verification enables MADDPG to simultaneously optimize multiple conflicting objectives while maintaining policy stability, confirming theoretical variance reduction guarantees derived in Theorems (1 & 2).

TABLE III
EFFECT OF PIS PARAMETERS

Configuration	Throughput (Mbps)	URLLC CR(%)	$\text{Var}(\hat{P}_f)$ ($\times 10^{-5}$)	Latency per user(ms)
Proposed ($\alpha = 0.6$)	3097	72	5.2	0.57
High α ($\alpha = 0.9$)	2219	50.6	29.8	0.42
Low α ($\alpha = 0.3$)	2376	52.8	19.1	0.64
Uniform ($N = 1000$)	2998	68.1	4.8	11

V. CONCLUSION

We presented a PIS based theoretically-grounded framework for sample-efficient coverage verification in multi-UAV networks. By combining LSTM-MDN trajectory prediction with defensive mixture importance sampling, we achieve provable variance reduction while maintaining unbiasedness. Integration with MADDPG enables real-time proactive control for multi-UAV trajectory planning. Experimental validation demonstrates the superiority of our proposed approach over existing approaches like vanilla MADDPG, SAC, MADDPG-BO and pure

uniform sampling. Future work includes adaptive mixture control (learning α online based on prediction uncertainty), extension to 3D mobility for aerial users, and hardware validation on real UAV testbeds. Moreover, the proposed PIS framework can be generalized beyond UAV networks to any mobile wireless system requiring sample-efficient spatial coverage verification.

REFERENCES

- [1] M. Mozaffari, W. Saad, M. Bennis, Y.-H. Nam, and M. Debbah, “A tutorial on UAVs for wireless networks: Applications, challenges, and open problems,” *IEEE Commun. Surveys Tuts.*, Vol. 21, No. 3, pp. 2334–2360, 2019.
- [2] W. Saad, M. Bennis and M. Chen, “A vision of 6G wireless systems: Applications, trends, technologies, and open research problems,” *IEEE Network*, Vol. 34, No. 3, pp. 134–142, 2020.
- [3] A. Al-Hourani, S. Kandeepan, and S. Lardner, “Optimal LAP altitude for maximum coverage,” *IEEE Wireless Commun. Lett.*, Vol. 3, No. 6, pp. 569–572, 2014.
- [4] Y. Zeng and R. Zhang, “Energy-efficient UAV communication with trajectory optimization,” *IEEE Trans. Wireless Commun.*, Vol. 16, No. 6, pp. 3747–3760, 2017.
- [5] M. Alzenad, A. El-Keyi, F. Lagum, and H. Yanikomeroglu, “3D placement of an unmanned aerial vehicle base station (UAV-BS) for energy-efficient maximal coverage,” *IEEE Wireless Commun. Lett.*, Vol. 6, No. 4, pp. 434–437, 2017.
- [6] X. Yan, A. Sekercioglu, S. Narayanan, “A survey of vertical handover decision algorithms in fourth generation heterogeneous wireless networks”, *Computer Networks*, Vol. 54, pp. 1848–1863, 2010.
- [7] D. Ravi and R. Arunachalam, “Optimizing UAV deployment for maximizing coverage and data rate efficiency using multi-agent deep deterministic policy gradient and Bayesian optimization,” *Phys. Commun.*, vol. 69, p. 102621, 2025.
- [8] R. Y. Rubinstein and D. P. Kroese, *Simulation and the Monte Carlo Method*, 3rd ed. Wiley, 2016.
- [9] A. B. Owen, *Monte Carlo Theory, Methods and Examples*. 2013.
- [10] M. R. Akdeniz, Y. Liu, M. K. Samimi, S. Sun, S. Rangan, T. S. Rappaport, and E. Erkip, “Millimeter wave channel modeling and cellular capacity evaluation,” *IEEE J. Sel. Areas Commun.*, Vol. 32, No. 6, pp. 1164–1179, 2014.
- [11] P. Qin, Y. Fu, Z. Yu, J. Zhang, X. Zhao, “URLLC-Aware trajectory plan and beamforming design for NOMA-aided UAV integrated sensing, communication, and computation Networks”, *IEEE Trans. on Veh. Tech.*, Vol. 74, pp. 1610-1625, 2025.
- [12] T. Yang, C. H. Foh, F. Heliot, C. Y. Leow, P. Chatzimisios, “Self-organization drone-based unmanned aerial vehicles (UAV) Networks”, *Proc. ICC*, pp. 1-6, 2019.
- [13] R. D. Kumar, A. Rammohan, “Optimizing UAV deployment for maximizing coverage and data rate efficiency using multi-agent deep deterministic policy gradient and Bayesian optimization”, *Physical Communication*, Vol. 69, 102621, 2025.
- [14] R. Lowe, Y. Wu, A. Tamar, J. Harb, P. Abbeel, I. Mordatch, “Multi-agent actor-critic for mixed cooperative-competitive environment”, *Proc. NIPS*, 6382–6393, 2017.
- [15] R. Y. Rubinstein and D. P. Kroese, *Simulation and the Monte Carlo Method*, 3rd ed. Wiley, 2017.
- [16] S. Hochreiter and J. Schmidhuber, “Long short-term memory,” *Neural Comput.*, Vol. 9, No. 8, pp. 1735–1780, 1997.
- [17] C. M. Bishop, “Mixture density networks,” Tech. Rep. NCRG/94/004, Aston Univ., 1994.
- [18] A. Alahi, K. Goel, V. Ramanathan, A. Robicquet, L. Fei-Fei, and S. Savarese, “Social LSTM: Human trajectory prediction in crowded spaces,” in *Proc. CVPR*, 2016, pp. 961–971, 2016.
- [19] N. Lee *et al.*, “DESIRE: Distant future prediction in dynamic scenes with interacting agents,” in *Proc. CVPR*, pp. 336–345, 2017.
- [20] F. Li, C. He, X. Li, J. Peng, and K. Yang, “Geometric analysis-based 3D anti-block UAV deployment for mmWave communications,” *IEEE Commun. Lett.*, Vol. 26, No. 11, pp. 2799–2803, 2022.
- [21] S. Parial, S. C. Ghosh and A. K. Ghosh, “User-UAV association for dynamic user in mmWave communication for eMBB and URLLC,” *Proc. SoftCOM*, pp. 1-16, 2025.